Nonlinear Dyn (2021) 105:2157–2172
https://doi.org/10.1007/s11071-021-06738-z

ORIGINAL PAPER

Parameter identification of nonlinear bistable piezoelectric structures by two-stage subspace method

Qinghua Liu · Junyi Cao · Fangyuan Hu · Dan Li · Xingjian Jing · Zehao Hou

Received: 4 March 2021 / Accepted: 14 July 2021 / Published online: 28 July 2021

Abstract System parameters identification of nonlinear bistable structures has attracted considerable interest because the performance enhancement of energy harvesting and vibration control is significantly dependent on the model parameter of nonlinear systems. Therefore, a two-stage subspace method is proposed to identify the critical parameters in the system equation of nonlinear bistable piezoelectric structures. The dynamic equation of nonlinear bistable piezoelectric structures is separated into an underlying linear electromechanical coupling equation and a nonlinear mechanical equation. At first, for the underlying linear electromechanical coupling equation, a force–displacement subspace is constructed to identify the linear mass, damping and stiffness. Meanwhile, a velocity–voltage subspace is created for the identification of the electromechanical coupling coefficient. Next, for the nonlinear mechanical equation, the nonlinear restoring force in bistable structures can be estimated by the extended nonlinear frequency response function. Numerical simulation on a magnetic coupled bistable piezoelectric structure is performed to investigate the influence of frequency-swept responses, the noise intensity and polynomial order on identification accuracy. Experimental measurement of a magnetic coupled asymmetric bistable piezoelectric beam is conducted under different excitation conditions. Experimental results demonstrate the effectiveness of the proposed identification method.

Keywords Bistable structures · Nonlinear parameter identification · Two-stage subspace method · Electromechanical coupling equation · Nonlinear restoring force

Q. Liu · J. Cao (✉) · F. Hu · D. Li · Z. Hou
Key Laboratory of Education Ministry for Modern Design and Rotor-Bearing System, School of Mechanical Engineering, Xi'an Jiaotong University, Xi'an 710049, China
e-mail: caojy@mail.xjtu.edu.cn

X. Jing
Department of Mechanical Engineering, The Hong Kong Polytechnic University, Hong Kong, China

1 Introduction

In the last decade, nonlinear piezoelectric structures have attracted a lot of interest in vibration energy harvesting, vibration absorption and actuation [1–4]. Among the investigations of favorable nonlinear piezoelectric structural designs and dynamics for improving energy harvesting capability, nonlinear bistable piezoelectric structures have been employed to exhibit large amplitude electromechanical dynamics under low-frequency vibration excitations [5, 6]. Generally, a nonlinear bistable piezoelectric structure incorporates a nonlinear restoring force using different design approaches, including magnetic levitation

[7, 8], axial loading [9, 10] and metamaterial structures coupling [11, 12], etc. These nonlinear elements can improve the operational frequency band and exhibit the non-resonant nature of snap-through dynamics. However, these nonlinear configurations may lead to the identification difficulty of critical parameters such as equivalent mass, damping coefficient, nonlinear restoring force, and electromechanical coupling coefficient.

In recent decades, much effort has been devoted to investigating the governing model derivation and the effect of system physical parameters and nonlinear restoring force. Erturk et al. investigated the governing lumped-parameter equation with the nonlinear restoring force for describing the dynamics of a magnetic buckling bistable piezomagnetoelastic generator [13]. Stanton et al. derived the dynamic model of the magnetic coupled bistable piezoelectric cantilever beam using the energy principles and magnetic dipoles theory [14]. Cao et al. experimentally measured the nonlinear restoring force in a rotatable magnetic coupled nonlinear bistable cantilever beam and then fitted it with a polynomial model [15]. Leadenham and Erturk et al. used force and displacement sensors to obtain force–displacement curves in an M-shaped piezoelectric energy harvesting device with a third-order polynomial [16] or a fifth-order polynomial [17]. Masana et al. proposed the system model of a clamped–clamped axially loaded bi-stable (post-buckling) piezoelectric beam based on Hamilton's principle, and their parameters were all calculated analytically [18]. Myungwon et al. presented a metamaterial-inspired bistable lattice, and its magnetic interaction force was measured and fitted with cubic force functions [11]. Among the above-mentioned nonlinear bistable structures, the critical parameters in the dynamical equation were obtained by theoretical calculation or quasi-static measurement. However, it will be difficult to calculate or characterize these parameters accurately due to the uncertainties of the bonding process of piezoelectric ceramics and clamping conditions of piezoelectric structures.

Additionally, another promising method of obtaining the model parameters is based on the system identification technology. Stanton et al. identified the model parameters of nonlinear piezoelectric structures via a nonlinear least-squares optimization algorithm that utilized the approximate analytic solution obtained by the harmonic balance method [19]. Zhou et al. employed a genetic algorithm to identify the equivalent damping coefficient and electromechanical coupling coefficient in a magnetic coupled tristable piezoelectric cantilever beam [20]. Yuan et al. addressed the hardening and softening nonlinearity in a circular laminated plate using the Hilbert transform-based method, and the strong nonlinearity of electrical parameters was estimated by the current mapping approach [21, 22]. Nico et al. and Harris et al. introduced signal decomposition methods, such as high-order spectral techniques [23] and wavelet analysis [24], to investigate the nonlinear responses of piezoelectric energy harvesting devices. In addition to the above signal processing and optimization methods, the time-domain nonlinear subspace method initially proposed by Marchesiello et al. [25] was employed to identify nonlinear restoring force [26]. Ghamami et al. proposed a two-stage automated identification algorithm based on data-driven stochastic subspace, classification, and clustering methods to estimate the modal parameters of bistable composite plates and concrete arch dam [27, 28]. The improved nonlinear frequency domain subspace algorithm has been widely used in aerospace structures such as impacts on the mechanical stops [29], bolted connected joints on wingtips [30] and solar array structures [31]. Moreover, some interesting improvements have been made in nonlinear beam identification. Liu et al. proposed the modified time-domain subspace method based on a nonlinear separation strategy which reduces the coupling error in the traditional nonlinear subspace method [32, 33]. Anastasio et al. proposed an ad hoc version of the nonlinear subspace identification algorithm in the reduced-order domain to identify distributed nonlinearities in a flexible beam structure [34]. However, there is rarely investigation into subspace parameter identification of bistable piezoelectric structures. These nonlinear bistable structures always exhibit more complicated dynamic phenomenon such as intra-well and inter-well chaos oscillation. Therefore, improper output response under a given excitation condition will result in unvalidatable identification. Besides, the nonlinear restoring force in many bistable structures cannot be exactly described using a polynomial expression due to measurement error or structural constraints. Therefore, in addition to parameter identification of nonlinear bistable structures, the influence of dynamic responses signal selection, noise level and polynomial

order on the identification process should be thoroughly investigated.

To address the above issues, a two-stage subspace method is proposed for the identification of equivalent mass, damping coefficient, linear stiffness, electromechanical coupling coefficient and nonlinear restoring force in a nonlinear bistable piezoelectric structure. The dynamical equation of bistable piezoelectric structures to be identified is separated into an underlying linear electromechanical coupling equation and a nonlinear mechanical equation. For the underlying linear electromechanical coupling equation, a force–displacement subspace is constructed to identify the linear mass, damping and stiffness, and a velocity–voltage subspace is proposed for the identification of the electromechanical coupling coefficient. For the nonlinear mechanical equation, the nonlinear restoring force in bistable structures can be estimated by the extended nonlinear frequency response function. Numerical simulations are conducted to investigate the identification performance. The frequency-swept response selection, noise pollution and the choice of polynomial order are also discussed. Moreover, experimental verification is conducted on a magnetic coupled bistable piezoelectric cantilever beam.

The paper is organized as follows. In Sect. 2, the nonlinear subspace identification process is introduced. And then in Sect. 3, the proposed two-stage subspace method for the identification of nonlinear bistable piezoelectric structures is presented. Section 4 is dedicated to the numerical validation and influence factors in the identification accuracy of the proposed method. Experimental verification and evaluation are performed in Sect. 5. Finally, the conclusion of the present study is summarized in Sect. 6.

2 Subspace identification for nonlinear system

2.1 Nonlinear state-space model

The governing equation of a nonlinear dynamical system with a single degree of freedom can be expressed in the following form [25]

$$M\ddot{q}(t) + C_v\dot{q}(t) + Kq(t) + \sum_{i=1}^{m} k_i L_{ni} q_i(t) = f(t) \quad (1)$$

where M, C_v and K are equivalent linear mass, viscous damping coefficient and stiffness, respectively; $q(t)$ and $f(t)$ are the response displacement and external excitation force, respectively. The nonlinear restoring force term can be described as the sum of m components, and each of them depends on the scalar nonlinear basis function $q_i(t)$ through a vector L_{ni}, which represents the position of the nonlinear element that can be assumed as 1, − 1 or 0 [25].

It is supposed that the original system can be subjected to the external excitation force $f(t)$ and an internal feedback force $\sum_{i=1}^{m} k_i L_{ni} q_i(t)$. This method has been used to derive the frequency domain method of "Nonlinear Identification through Feedback of the Outputs" and is also based on the current time-domain identification method [35]. By moving the nonlinear restoring force term of Eq. (1) to the right-hand side of the function, Eq. (1) can be rewritten as

$$M\ddot{q}(t) + C_v\dot{q}(t) + Kq(t) = f(t) - \sum_{i=1}^{m} k_i L_{ni} q_i(t) \quad (2)$$

The deterministic subspace method computes the state space equations from input force and output displacement data sets. So, the dynamic equation in Eq. (2) can be transformed into a state-space model. Since the displacement can be measured and velocity can be obtained by differential procedure, the state vector $x = (q^T, \dot{q}^T)^T$ and an input force vector $u = [f(t) - q_1(t) - q_2(t) \cdots - q_m(t)]^T$ are defined. Then, the state-space formulation of Eq. (2) is given as

$$\begin{cases} \dot{x}(t) = A_c x(t) + B_c f(t) + B_c^{nl} q(t) \\ q(t) = C_c x(t) + D_c f(t) \end{cases} \quad (3)$$

where subscript c stands for continuous-time, A_c, B_c,B_c^{nl}, C_c, D_c are dynamical system, input, nonlinear feedback input, output and direct feed-through matrices, respectively. The state-space matrix and the physical space equation should meet

$$A_c = \begin{bmatrix} 0 & I \\ -M^{-1}K & -M^{-1}C_v \end{bmatrix};$$
$$B_c^{nl} = \begin{bmatrix} 0 & \cdots & 0 \\ M^{-1}u_1 L_{n1} & \cdots & M^{-1}u_m L_{nm} \end{bmatrix}$$
$$B_c = \begin{bmatrix} 0 \\ M^{-1} \end{bmatrix}; \quad C_c = [I \quad 0]; \quad D_c = [0 \quad 0 \quad \cdots \quad 0] \quad (4)$$

The continuous model can be transformed into a discrete state-space model by assuming zero-order holds for the input $f(t)$. A discrete-time translation of Eqs. (3) is eventually considered as

$$\begin{cases} x(\tau+1) = A_d x(\tau) + B_d^e e(y(\tau), u(\tau)) \\ y(\tau) = C_d x(\tau) + D_d^e e(y(\tau), u(\tau)) \end{cases} \tag{5}$$

where τ is the sampled time, subscript d stands for discrete-time and $B_d^e = (B_d\ B_d^{nl})$.

2.2 Subspace identification process

The class of subspace identification algorithms [36] aims to estimate the discrete-time deterministic state-space model by measured inputs and outputs. Iterating the two Eqs. (5) yields

$$\begin{aligned} y(\tau) = {} & C_{\mathrm{d}} A_d^{\tau} x(0) + C_{\mathrm{d}} A_d^{\tau-1} B_d u(0) \\ & + C_{\mathrm{d}} A_d^{\tau-2} B_d u(1) + \cdots \\ & + C_{\mathrm{d}} A_d^{\tau-2} B_d u(\tau-1) + D_{\mathrm{d}} u(\tau) \end{aligned} \tag{6}$$

For identifying the matrices A_d, B_d, C_d and D_d, the so-called extended observability matrix Γ_u is defined as

$$\Gamma_u = \left(C^T\ (CA)^T\ (CA^2)^T \cdots (CA^{u-1})^T\right)^T \tag{7}$$

and the lower block triangular Toeplitz matrix Λ_u is defined as

$$\Lambda_u = \begin{pmatrix} D^e & 0 & 0 & \cdots & 0 \\ CB^e & D^e & 0 & \cdots & 0 \\ CAB^e & CB^e & D^e & \cdots & 0 \\ \vdots & \vdots & \vdots & & \vdots \\ CA^{u-2}B^e & CA^{u-3}B^e & CA^{u-3}B^e & \cdots & D^e \end{pmatrix} \tag{8}$$

In the subspace identification method, the introduction of Block Hankel matrices is very important. If the displacement response and input force to the system can be easily measured, then extended input block Hankel matrix and output Hankel matrix can therefore be defined as

$$\begin{cases} E_u = \left[u_{0:l-1}^T\ \ u_{1:l}^T \cdots u_{h-1:h+l-2}^T\right] \\ Y_u = \left[y_{0:l-1}^T\ \ y_{1:l}^T \cdots y_{h-1:h+l-2}^T\right] \end{cases} \tag{9}$$

where h is a user-defined number representing half the number of rows and l denotes the number of columns in the input block Hankel matrix.

If Eqs. (7–9) are recursively substituted to Eq. (6), it can provide the following matrix equation

$$Y_u = \Gamma_u x + \Lambda_u E_u \tag{10}$$

It should be noted that the specific geometric manipulation of the row spaces of the above matrix can refer to Ref. [25] to obtain the system properties. It will not be discussed in this paper. So far, many algorithms had been developed to estimate the state space matrics, such as N4SID [37], MOESP [38] and PEM [39]. In this paper, the N4SID is adopted, which had already integrated into MATLAB. Once the *A, B, C, D* in the spate-space model are identified, the final step is to estimate linear coefficient K and nonlinear coefficients k_i by the frequency response function of the underlying linear system and extended nonlinear frequency response function, respectively. The underlying linear system acceptance matrix can be obtained by taking the Fourier transform of the linear state-space model

$$H(\omega) = \left(-\omega^2 M + j\omega C_v + K\right)^{-1} \tag{11}$$

It had been mentioned above that the nonlinear restoring force could be treated as an internal nonlinear feedback force as shown in Eq. (2). By taking the Fourier transform, the frequency domain version of the Eq. (2) is

$$H^{-1}(\omega) Q(\omega) = F(\omega) - \sum_{i=1}^{m} k_i Q_i(\omega) L_{ni} \tag{12}$$

where $Q(\omega)$, $Q_i(\omega)$ and $F(\omega)$ are Fourier transforms of $q(t)$, $q_i(t)$ and $f(t)$, respectively. Therefore, the relationship between the nonlinear frequency response function and the underlying linear system frequency response function is

$$H_e(\omega) = H(\omega)\left[K^{-1}\ K^{-1}k_1 L_{n1}\ K^{-1}k_2 L_{n2} \cdots\ K^{-1}k_m L_{nm}\right] \tag{13}$$

By assuming the ω = 0, the final nonlinear coefficients in restoring force function can be obtained based on Eq. (13).

Besides, the basic physical parameters including undamped circular eigenfrequency ω_{un} and damping ratio ξ can be estimated through the eigenvalue decomposition of the estimated system matrix A [40].

$$\omega_{un} = \sqrt{\lambda_R^2 + \lambda_I^2}; \quad \xi_i = \frac{|\lambda_R|}{\sqrt{\lambda_R^2 + \lambda_I^2}} \tag{14}$$

where λ_R and λ_I are two eigenvalues. Then the equivalent mass can be estimated by $M = K/\omega_{un}$.

3 Two-stage identification for piezoelectric bistable structures

3.1 Modeling of piezoelectric bistable beam

It is widely known that nonlinear bistable piezoelectric structures have two stable equilibrium positions and one unstable equilibrium position as shown in Fig. 1. The configuration is composed of a spring steel substrate, two lead zirconate titanate (PZT5) piezoelectric layers bonded near the root, along with two tip magnets and two external rotatable magnets. Due to the interaction between the end magnets with the rotatable magnets, the nonlinear stiffness force becomes nonlinear and the bistable case is a very typical one that will be studied in this paper.

Based on the Euler–Bernoulli beam theory, discretization method and Hamilton principle, the equivalent lumped electromechanical dynamic modeling of the nonlinear bistable piezoelectric cantilever beam can be expressed as [41]

$$\begin{cases} M\ddot{x}(t) + C_v\dot{x}(t) + Kx(t) + F_n(t) - \theta v(t) = F(t) \\ \theta\dot{x}(t) + C_p\dot{v}(t) - v(t)/R = 0 \end{cases} \tag{15}$$

where M, C_v, K, $F_n(t)$ are the equivalent mass, linear damping coefficient, linear stiffness and the nonlinear coupled magnetic force, respectively. θ is the equivalent electromechanical coupling coefficient; C_p is the equivalent capacitance of the piezoelectric layer; R is the load resistance; $v(t)$ is the voltage across the electrical load; $x(t)$ is the tip displacement of the beam in the transverse direction; and $F(t)$ is the external excitation force in the beam thickness direction.

To understand the dynamic characteristics, the value of parameters M, C_v, K, $F_n(t)$, θ, C_p in Eq. (15) should be identified. It is also found that the value of $F_n(t)$ and θ are the most difficult parameters to be accurately calculated or directly measured. Moreover, in most previous studies, the vicious damping C_v, linear stiffness K and equivalent capacitance C_p are the same as the underlying linear piezoelectric beam system [22, 42, 43]. Therefore, the nonlinear magnetic coupling electromechanical equation can be separated into two parts for parameter identification. The more specific identification steps will be performed in the following section.

3.2 Two-stage identification based on subspace method

3.2.1 First stage: identify underlying linear electromechanical system

When the external magnets are removed, the structure will become a simple linear piezoelectric beam. It means the $F_n(t)$ in Eq. (15) does not exist. Converting this continuous second-order differential equation to state-space equation by choosing the state vector as $x = [x(t)\ \dot{x}(t)\ v(t)]^T$, input vector as $[F(t)]$, and output vector as $y = [x(t)\ v(t)]^T$, it has

$$\begin{cases} \begin{bmatrix} \ddot{x}(t) \\ \dot{x}(t) \\ \dot{v}(t) \end{bmatrix} = \begin{bmatrix} 0 & 1 & 0 \\ -\dfrac{K}{M} & -\dfrac{C_v}{M} & \dfrac{\theta}{M} \\ 0 & -\dfrac{\theta}{C_p} & -\dfrac{1}{RC_p} \end{bmatrix} \begin{bmatrix} x(t) \\ \dot{x}(t) \\ v(t) \end{bmatrix} + \begin{bmatrix} 0 \\ 1 \\ 0 \end{bmatrix} [F(t)] \\ \begin{bmatrix} x(t) \\ v(t) \end{bmatrix} = \begin{bmatrix} 1 & 0 & 0 \\ 0 & 0 & 1 \end{bmatrix} \begin{bmatrix} x(t) \\ \dot{x}(t) \\ v(t) \end{bmatrix} \end{cases} \tag{16}$$

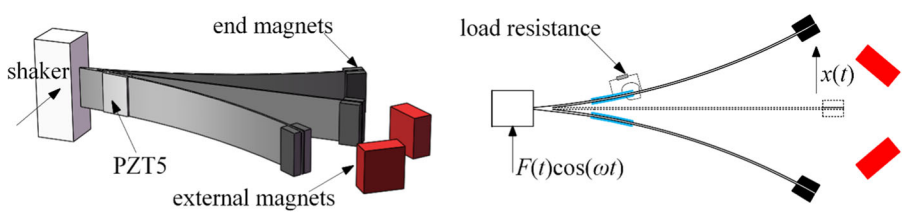

Fig. 1 Schematic diagram of nonlinear bistable piezoelectric structures

Then, Eq. (16) is decomposed into two subsystems, named as force–displacement subsystem and velocity–voltage subsystem shown in Eq. (17) and Eq. (18), respectively.

$$\begin{cases} \begin{bmatrix} \ddot{x}(t) \\ \dot{x}(t) \end{bmatrix} = \begin{bmatrix} 0 & 1 \\ -\dfrac{K}{M} & -\dfrac{C_v}{M} \end{bmatrix} \begin{bmatrix} x(t) \\ \dot{x}(t) \end{bmatrix} + \begin{bmatrix} 0 \\ \dfrac{1}{M} \end{bmatrix} [F] \\ x = [\,1 \quad 0\,] \begin{bmatrix} x(t) \\ \dot{x}(t) \end{bmatrix} \end{cases} \tag{17}$$

$$\begin{bmatrix} \dot{v}(t) \\ v(t) \end{bmatrix} = \begin{bmatrix} -\dfrac{\theta}{C_p} & -\dfrac{1}{RC_p} \\ 0 & 1 \end{bmatrix} \begin{bmatrix} \dot{x}(t) \\ v(t) \end{bmatrix} \tag{18}$$

Assuming that $\omega = 0$, the underlying linear system acceptance matrix for Eq. (17) is

$$\begin{aligned} H_{l1}(0) &= D_{l1} - C_{l1}A_{l1}^{-1}B_{l1} \\ &= [0] - [\,1 \quad 0\,] \begin{bmatrix} 0 & 1 \\ -\dfrac{K}{M} & -\dfrac{C_v}{M} \end{bmatrix}^{-1} \begin{bmatrix} 0 \\ \dfrac{1}{M} \end{bmatrix} \\ &= \begin{bmatrix} \dfrac{1}{K} \end{bmatrix} \end{aligned} \tag{19}$$

where subscript $l1$ denotes the identified frequency response function of the force–displacement subsystem. The linear stiffness can be obtained using the linear frequency response function. The equivalent mass and damping need to be identified by using the eigenvalue decomposition of matrix A_{l1}.

Similarly, the electromechanical coupling coefficient θ can be identified using the frequency response function of the velocity–voltage subsystem.

$$H_{l2}(0) = D_{l2} - C_{l2}A_{l1}^{-1}B_{l2} = -R\theta \tag{20}$$

where subscript $l2$ denotes the identified matrics of the velocity–voltage subsystem.

3.2.2 *Second stage: identify the nonlinear restoring force*

In Eq. (15), linear stiffness force and nonlinear magnetic force are coupled together, called nonlinear restoring force. The reaction force of the piezoelectric layer $\theta v(t)$ can be neglected because of a small order of magnitude. Moreover, the restoring force in a bistable piezoelectric cantilever beam can often be expressed as a polynomial model $F_n(t) = \sum_{i=1}^{m} k_i L_{ni} x^i(t)$. Here, the identification of nonlinear restoring force in a bistable electromechanical coupling system can be simplified into a bistable mechanical system, the substitution of $F_n(t) = \sum_{i=1}^{m} k_i L_{ni} x^i(t)$ into Eq. (2) gives

$$\begin{aligned} M\ddot{q}(t) + C_v\dot{q}(t) = f(t) &- (K + k_1)L_{n1}q(t) \\ &- \sum_{i=2}^{m} (k_2)L_{ni}q(t) \end{aligned} \tag{21}$$

The extended nonlinear frequency response function of the bistable piezoelectric cantilever beam is

$$H_n(\omega) = H_{l1}(\omega)[K \;\; k_1L_{n1} \;\; k_2L_{n2}\ldots k_mL_{nm}] \tag{22}$$

Finally, the nonlinear restoring force can be expressed by assuming the $\omega = 0$,

$$\begin{aligned} F_n(t) = &\left(\frac{1 + H(2)}{H(1)}\right)x + \left(\frac{H(3)}{H(1)}\right)x^2 \\ &+ \cdots \left(\frac{H(m)}{H(1)}\right)x^m \end{aligned} \tag{23}$$

It should be noted that this two-stage time-domain subspace method is applicable for a variety of nonlinear piezoelectric structures as long as the mechanical equation can be separated from the electromechanical coupling equation. For a clear understanding of the proposed two-stage time-domain subspace method, the identification flowchart of critical parameters in bistable piezoelectric structures is diagramed in Fig. 2.

4 Numerical investigation

In this section, the nonlinear bistable piezoelectric cantilever beam is illustrated for numerical verification of the proposed identification method. Besides, numerical simulation has been employed to study the influence of frequency-swept response signals and noise levels on the identification results. Finally, the choice of polynomial order of nonlinear restoring force will also be investigated.

In the numerical simulation, the equivalent mass, damping coefficient, linear stiffness, electromechanical coupling coefficient are 0.01 kg, 0.03 N/(m/s), 140 N/m, and 4×10^{-6} N/V, respectively. The coupled nonlinear restoring force function is $F_n = -170x + 750x^2 - 3 \times 10^5 x^3$. So, the governing

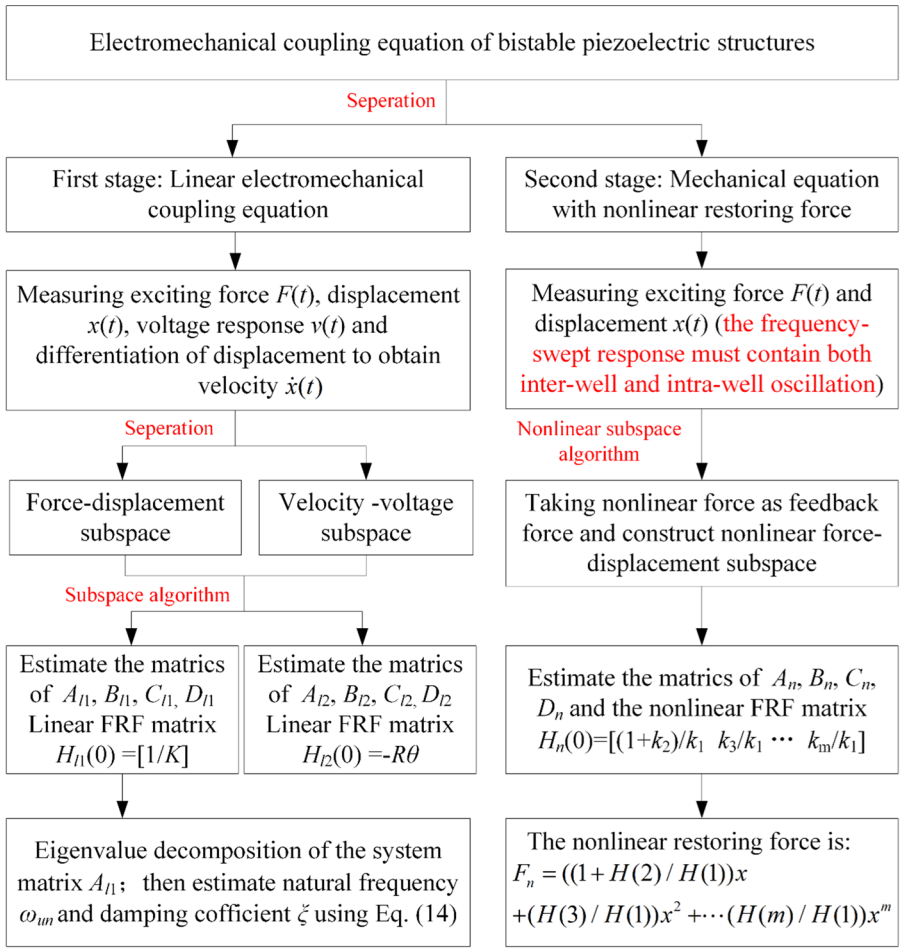

Fig. 2 A schematic diagram of the two-stage nonlinear subspace identification method

equation of the nonlinear bistable piezoelectric cantilever beam is

$$\begin{cases} 0.01\ddot{x}(t)+0.03\dot{x}(t)-30x+750x^2+3\times10^5x^3-4\times10^{-6}v(t)=F(t) \\ 4\times10^{-6}\dot{x}(t)+5\times10^{-9}\dot{v}(t)-v(t)/10^7=0 \end{cases} \tag{24}$$

The exciting force is a frequency-swept sine sequence, and the classical fourth-order Runge–Kutta algorithm is applied to obtain the dynamic responses of the simulation model described by Eq. (24). Furthermore, the measured response is inevitably polluted by noise in practice. All simulated input force and output displacement responses are added by an additive white noise with SNR = 40 dB (Signal Noise Ratio, SNR).

According to Sect. 3, the underlying linear electromechanical coupling system is extracted and separated into two subsystems. Firstly, linearly increasing frequency force excitation is performed over the frequency range of 10–30 Hz with an amplitude of 0.06 N. Then, numerical integration of the equation of motion has been performed, and 20,000 samples have been generated and adopted for the system identification. The excitation force and dynamic displacement response, and identified linear stiffness force are depicted in Fig. 3. The estimated mean value of linear stiffness K is 141.14 N/m which means the identification accuracy is 99.2%. Moreover, the mass and viscous damping coefficient are identified by carrying out eigenvalue decomposition of the identified system matrix A_{l1} and the results are 0.0107 kg and 0.0308 N/(m/s). By comparing with the mass and damping used in the simulation, the

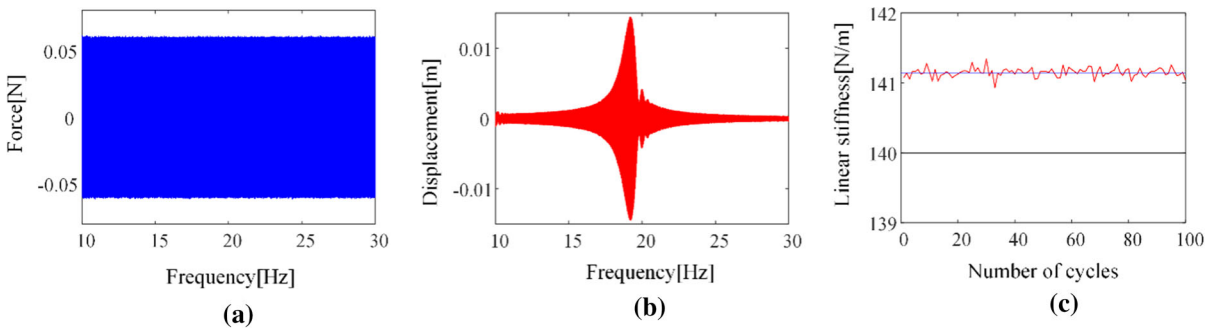

Fig. 3 Simulated identification data sets: **a** input force data under 40 dB noise; **b** output displacement response under 40 dB noise; **c** the identified linear stiffness with 100 Monte Carlo experiments for each simulation (red line); the mean value is 141.14 N/m plotted in blue line, and the black line is the theoretical value

identification accuracy is 93% and 97.3%, respectively.

For the velocity–voltage subsystem, the input and output identification data sets are velocity and voltage, as shown in Fig. 4. Similarly, the 40 dB white noise is added to the data sets. Using the identification method described in Sect. 3, the final estimated mean value of electromechanical coupling coefficient θ is 3.85×10^{-6} N/V, and accuracy is 96.3% compared to the theoretical results.

From the above investigated, the identification of basic mechanical and electrical parameters of linear piezoelectric cantilever beam can always keep a good identification ability by utilizing the proposed subspace-based method. However, in the second stage, identifying nonlinear restoring force function is not an easy task because of complicated dynamic response in the bistable system, the sensitivity to noise, and the uncertainness of polynomial order of nonlinear restoring force. Therefore, the choice of different types of dynamic displacement response and polynomial order will be discussed as follows.

4.1 The influence of dynamic response on identification

It is widely known that the bistable beam can exhibit typical inter-well and intra-well chaos oscillations. Generally, a frequency-swept excitation strategy is employed to study their dynamic response and system characteristics. In this section, linearly increasing frequency (up-sweep) excitation over the frequency range of 10–30 Hz in 40 s and the excitation force values is 0.12 N. The initial position of the oscillator is the stable equilibrium point of 0.008 m, and velocity is 0 m/s. Then, the same decreasing frequency (down-sweep) excitation is followed. As shown in Fig. 5a, the red line represents the displacement response in the first 40 s. It can be observed that the bistable beam keeps oscillating across the potential wells in the whole frequency-swept and a jump-down phenomenon occurs around 22 s. For decreasing frequency excitations, the dynamic response trajectories are plotted in the blue line. The bistable beam's dynamical response exhibits intra-well oscillation around 0.008 m, followed by an intra-well oscillation in another equilibrium point and finally oscillating across the two potential wells. The difference between the two displacement response trajectories is that the double-well characteristics can be easily found in the blue line. To investigate the influence of dynamic response data sets selection on identification accuracy, the above-mentioned data sets are adopted in the identification process, and the results are shown in Fig. 5b. The root-mean-square (RMS) error is adopted to evaluate the identification accuracy, as detailed in Table 1. The identified nonlinear restoring force curve based on data sets 1 has a higher error accuracy (14.04%) than data sets 2 (4.27%). So, it is found that a reasonable excitation force and frequency range should be selected to improve the identification accuracy. Numerical results shown in Fig. 5 indicate that the dynamical response of nonlinear bistable structures exhibiting both inter-well and intra-well oscillation is better than an inter-well motion for the proposed identification method.

For nonlinear restoring force identification of bistable structures, the great difficulty may come from identifying nonlinear restoring force between two bistable potential wells. In order to obtain the

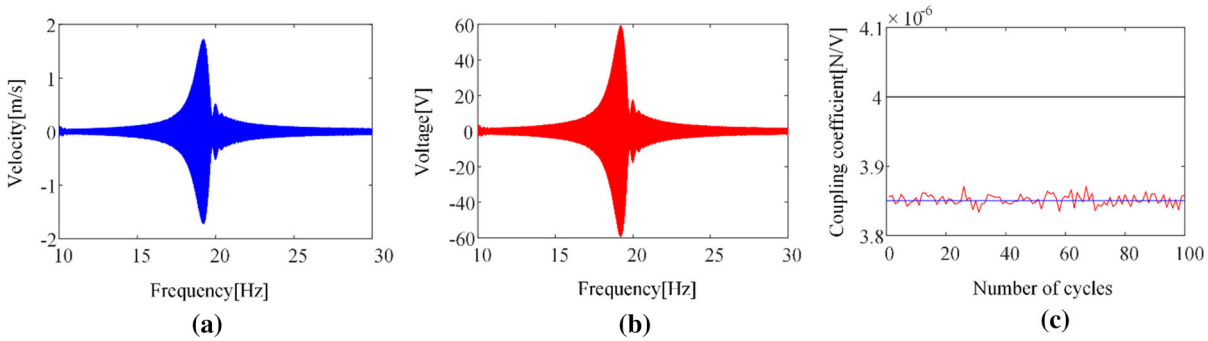

Fig. 4 Simulated identification data sets: **a** input velocity data under 40 dB noise; **b** output voltage response under 40 dB noise; **c** the identified electromechanical coupling coefficient with 100 Monte Carlo experiments for each simulation (red line); the mean value has 3.85×10^{-6} N/V plotted in the blue line, and the black line is the theoretical value

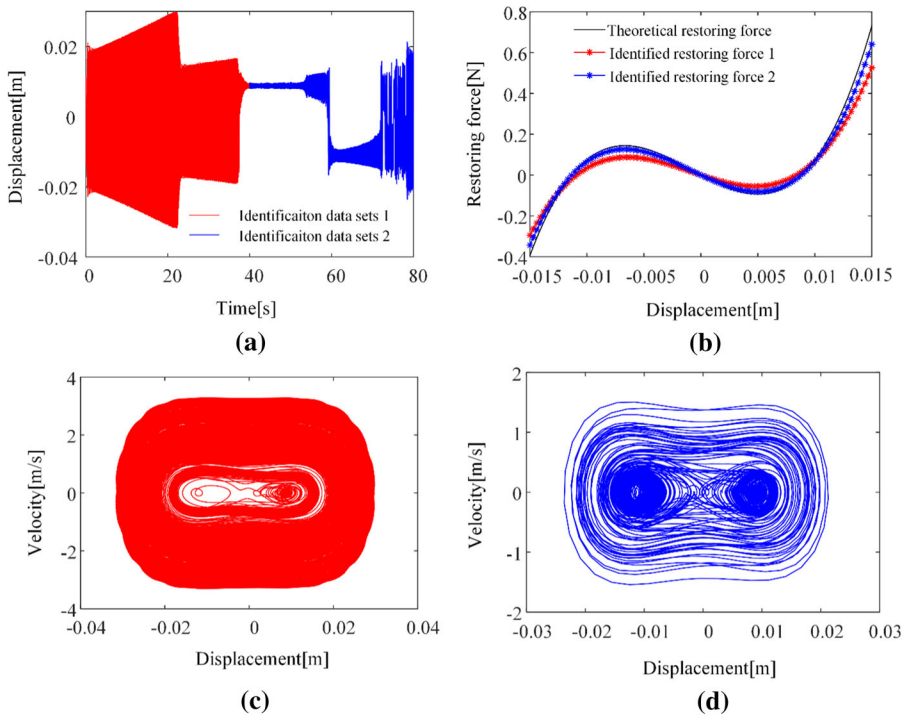

Fig. 5 Simulated identification data sets 1 (red line represents the forward sine sweep) and data sets 2 (blue line represents backward sine sweep) with a sampling frequency of 500 Hz: **a** output displacement response under 40 dB noise; **b** the identified restoring force curves based on two identification data sets with 100 Monte Carlo experiments for each simulation; **c** phase diagram of data sets 1; **d** phase diagram of data sets 2

Table 1 RMS error of identified nonlinear restoring force curves

Data sets	Inter-well oscillation	Inter-well and intra-well oscillation
Error (%)	14.04	4.27

nonlinear restoring force between two potential wells, the selected dynamical response need to reflect the oscillation characteristics of this displacement interval. In Fig. 5a, data sets 1 show fast jumping from -0.015 to $+0.015$ m, and it would lose the vibration characteristics of nonlinear restoring force

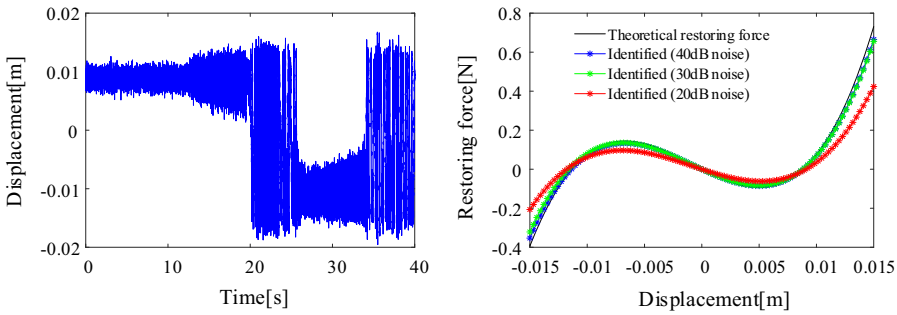

Fig. 6 **a** Output displacement response with a sampling frequency of 500 Hz (containing both intra-well oscillation and inter-well oscillation) under 20 dB noise; **b** comparison between the identified nonlinear restoring force curves: 20 dB noise (red line); 30 dB noise (green line); 40 dB noise (blue line) and the theoretical restoring force (black line)

driving. In Fig. 5c, the phase diagram of data sets 1 indicates that the phase space is incomplete in the small displacement region near two potential energy wells. Besides, the kind of large-amplitude oscillation is not unique to the bistable oscillator. For example, the hard stiffness spring or tristable oscillators can produce similar oscillations. On the contrary, it can be observed from data sets 2 that the oscillation trajectories show sufficient oscillations at two stable equilibrium points. It can be observed from Fig. 5d, the trajectory of data sets 2 almost covers the phase space. From the perspective of the identification algorithm, displacement and velocity are two significant elements for data-driven identification. The dynamic response of the oscillator must cover the phase space as much as possible.

4.2 The influence of noise pollution on identification

The above-investigated identification cases are only polluted by SNR = 40 dB noise. To deeply understand the robustness of the proposed method for nonlinear restoring force identification, SNR = 40 dB, 30 dB and 20 dB noise are added to the input and output data sets for identification comparison, respectively. According to Sect. 4.1, it is better to choose the identification data sets containing intra-well and inter-well oscillation. So, a new frequency-swept excitation is chosen for accurate identification and also for verification that the identification data sets used in Sect. 4.1 are not a special case. Figure 6a shows the dynamic response under the noise level of 20 dB. Although it is different from the trajectory of the oscillator in Sec. 4.1, it also includes both inter-well and intra-well motion. In Fig. 6b, the identification results show that the identification accuracy gradually decreases with the increase of noise intensity level and the RMS error is 0.55%, 3.31% and 14.9%, as detailed in Table 2, respectively. Moreover, relatively good identification results can be obtained under the noise level of 30 dB, but the error will be sharply increased if the data sets are polluted by noise exceeding 20 dB.

Table 2 RMS error of identified nonlinear restoring force curves

Noise level	40 dB	30 dB	20 dB
Error (%)	0.55	3.31	14.9

4.3 The influence of polynomial order on identification

In simulation examples, the function of the nonlinear restoring force is deterministic. This means the choice of polynomial order of nonlinear restoring force in the identification process does not influence identification results. In Fig. 7a, the same data sets in Sect. 4.2 were chosen excepted the noise level reduced to 40 dB. Figure 7b shows the comparison of identified nonlinear restoring force curves using different polynomial orders and the detailed estimated errors are given in Table 3. It can be observed that the identification accuracy has no significant difference though with the increase of polynomial order, the error increases slightly. It means the subspace algorithm can estimate

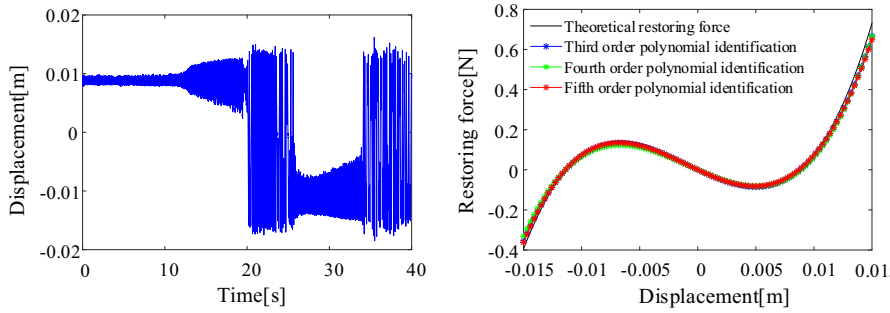

Fig. 7 Simulated output displacement response under 40 dB noise with a sampling frequency of 500 Hz; **b** comparison between the identified nonlinear restoring force by adopting different polynomial functions

Table 3 RMS error of identified nonlinear restoring force curves

Order	Third	Fourth	Fifth
Error (%)	3.53	4.95	6.47

the main nonlinear contributions from the original nonlinear basis functions, and polynomial order higher than third order will be assigned a small coefficient so that it does not affect the final restoring force function [34]. However, in practice, an optimal choice of polynomial order may be necessary because the nonlinear restoring force in a bistable structure is not a perfect polynomial form with a fixed order. In general, an approximate polynomial form is used to facilitate dynamic analysis. So, the identification process needs to find an optimal polynomial that can better characterize the nonlinear restoring force, and it will be thoroughly discussed in experimental conditions.

5 Experimental validation

An experimental test rig is set up in Fig. 8a to verify the two-stage subspace method for identifying bistable piezoelectric structures. The bistable piezoelectric cantilever beam is designed in the system with rotatable magnets coupling function. The excitation source is generated by a vibration exciter (JZK-50, Econ Technologies Co., Ltd), a power amplifier (YE5874A, Econ Technologies Co., Ltd), and a vibration controller (VT-9002-1, Econ Technologies Co., Ltd) is used to realize the feedback and real-time control of excitation signal. An acceleration sensor (CXL10GP3, MEMSIC., Inc) and a displacement sensor (HL-G112-A-C5, Keyence) are applied to record the excitation acceleration data and measure the absolute displacement response, respectively, and the data sets are collected by an oscilloscope (TBS2000, Tektronix) with probe resistance of 10MΩ. The middle elastic substrate used in the experiments is made of spring steel with dimensions $160 \times 15 \times 0.8\text{mm}^3$. Two piezoelectric layers made of PZT5 have a dimension of $15 \times 15 \times 0.6\text{mm}^3$. Two tip magnets have a dimension of $10 \times 10 \times 5\text{mm}^3$, and the two external rotatable magnets have a diameter of 10 mm and a thickness of 10 mm.

Another nonlinear stiffness force measurement experimental setup is shown in Fig. 8b. The Force Gauge (M5-2, MARK-10 Corporation) is installed on the structure driven by the ball screw and has an accuracy of 0.002 N. As the dynamometer pushes the cantilever beam to deform, the movement displacement will be recorded by Digital Indicator. Each measurement needs to be carried out from the steady-state point position and then arrange the force–displacement data from negative to positive deflection. This means the number of measurements is divided into four segments in the asymmetric bistable piezoelectric beam. The final nonlinear restoring force function can be obtained by polynomial fitting of the measured force–displacement trajectory.

The first step aims to estimate the mass, linear stiffness, damping coefficient, and electromechanical coupling coefficient. An acceleration sensor is arranged in experimental conditions instead of a force sensor, so a time-domain attenuation method is adopted here. Firstly, a linear piezoelectric cantilever beam was pushed to a specific position and then released. The natural frequency f_n = 18.5 Hz can be

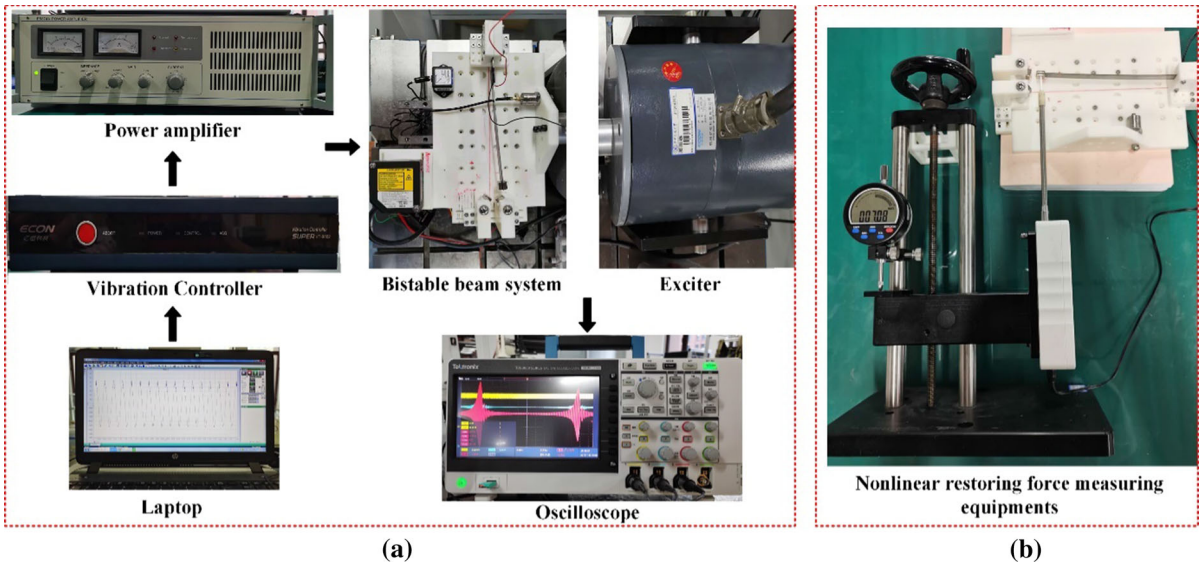

Fig. 8 Experimental setup. **a** Excitation control, piezoelectric bistable beam fixture and data acquisition system; **b** nonlinear restoring force measuring equipment

estimated by checking the number of oscillations in one second. The linear stiffness K = 140 N/m was measured by using the static measurement instruments. Then, the mass M can be calculated through the formula $M = K/(2\pi f_n)^2 = 10.36 \times 10^{-3}$ kg. In the following frequency-sweeping experiments, the input force is replaced by the equivalent mass multiplied by the measured acceleration.

A forward sine sweep followed by a backward sine sweep signal excitation is adopted to construct the identification data sets in two subspaces. The excitation acceleration amplitude is 3 m/s^2 with a frequency range of 8–23 Hz. Figure 9 shows the input acceleration, displacement response, and output voltage response after noise filtering (Butterworth low-pass filter with frequency 100 Hz). The mass M = 0.0108 kg, damping coefficient C_v = 0.0143 N/(m/s) and stiffness K = 151.52 N/m are identified by constructing force–displacement subsystem and then make subspace identification procedure. The value of the electromechanical coupling coefficient $\theta = 1.3 \times 10^{-6}$ N/V is estimated in the velocity–voltage subsystem. The equivalent capacitance coefficient $C_p = 4.2 \times 10^{-10}$F can be easily obtained from related theory once the electromechanical coupling coefficient is already identified.

It is not easy to compare the identified value with the theoretical value in experimental conditions due to the unknown parameters in the piezoelectric cantilever beam. Generally, the identified parameters are substituted into the original equation and then reconstruct the dynamical response. In Fig. 10, the displacement response and voltage response under the excitation of the same signal used in identification are compared. Figure 10a, b shows that the reconstructed dynamic response can keep a good agreement with the experimental measurement one though the identified natural frequency is a little higher.

In the second step, the goal is to identify the nonlinear restoring force in a magnetic coupled piezoelectric cantilever beam. Figure 11a shows the displacement response of the bistable beam under the swept-frequency excitation (8–23 Hz forward sweep followed a 23–8 Hz backward sweep). The base acceleration is 5.5 m/s^2, and the swept time is 60 s. It can be observed that the beam keeps increasing its amplitude across the potential wells until a jump-down phenomenon occurs around 20 s. This kind of response is adopted in the subspace-based nonlinear subspace algorithm, and the results are depicted in Fig. 11b. The nonlinear restoring force function is recognized as only hard spring characteristics and the negative stiffness zone have been missed. This kind of phenomenon has also been discussed in numerical examples and verified again in these experiments. In the following frequency-swept experiments, the

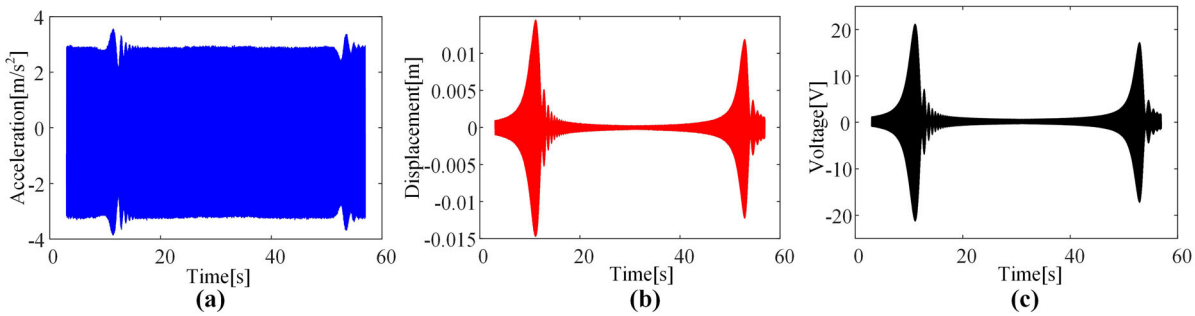

Fig. 9 Experimental identification data sets with a sampling frequency of 3125 Hz in a linear piezoelectric cantilever beam. **a** Input acceleration; **b** displacement response; **c** voltage response

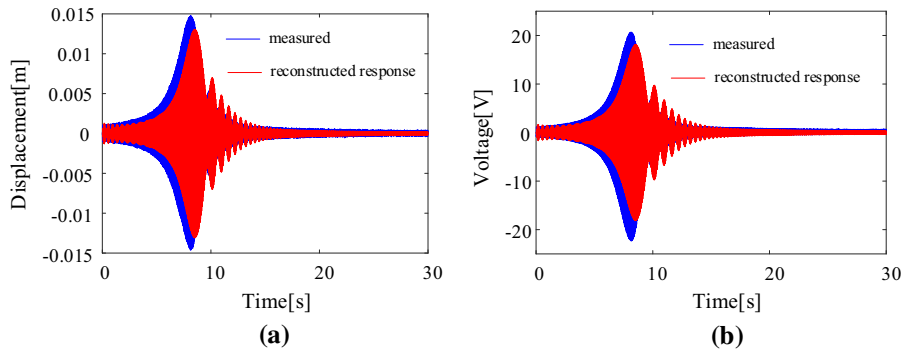

Figure 10 **a** Displacement response comparison between the measured (blue line) and reconstructed (red line); **b** voltage response comparison between the measured (blue line) and reconstructed (red line)

excitation acceleration is reduced to 5 m/s^2 and keeps other parameters unchanged. Figure 11c shows the experimental response of the bistable beam in this case. It can be found from Fig. 11c that the piezoelectric beam exhibits intra-well oscillation in two potential wells in the most swept time except two inter-well oscillations around 16 s and 48 s. The measured force–displacement trajectory and identified nonlinear restoring force curves are plotted in Fig. 11d, and RMS errors are listed in Table 4. The estimated third-order and fifth-order polynomial models have good accuracy with the measured results. Moreover, the error of three polynomial models increases gradually when the oscillator exhibits large displacement. It should be noted that measured force–displacement trajectory and identified results are disturbed by various noises and errors. Moreover, the dynamic response of a bistable system is very sensitive to excitation conditions. So, the reconstructed dynamic response results of the two methods will not be compared and discussed here.

6 Conclusions

This paper proposed a two-stage subspace method to identify the critical parameters in the dynamical equation of nonlinear bistable piezoelectric structures. The challenges of accurately identifying bistable structures persist because the jumping phenomenon between two potential wells, uncertainty polynomial form of nonlinear restoring force, and high noise level are unavoidable. The proposed identification algorithm is based on the separation of nonlinear electromechanical coupling equations into underlying linear electromechanical coupling equations and a nonlinear mechanical equation. At first, the basic physical parameters of the bistable piezoelectric beam can be estimated through underlying linear force–displacement subspace and voltage–velocity subspace. Next, the nonlinear force–displacement subspace can identify the nonlinear restoring force parameters. Thus, the separation and step-by-step

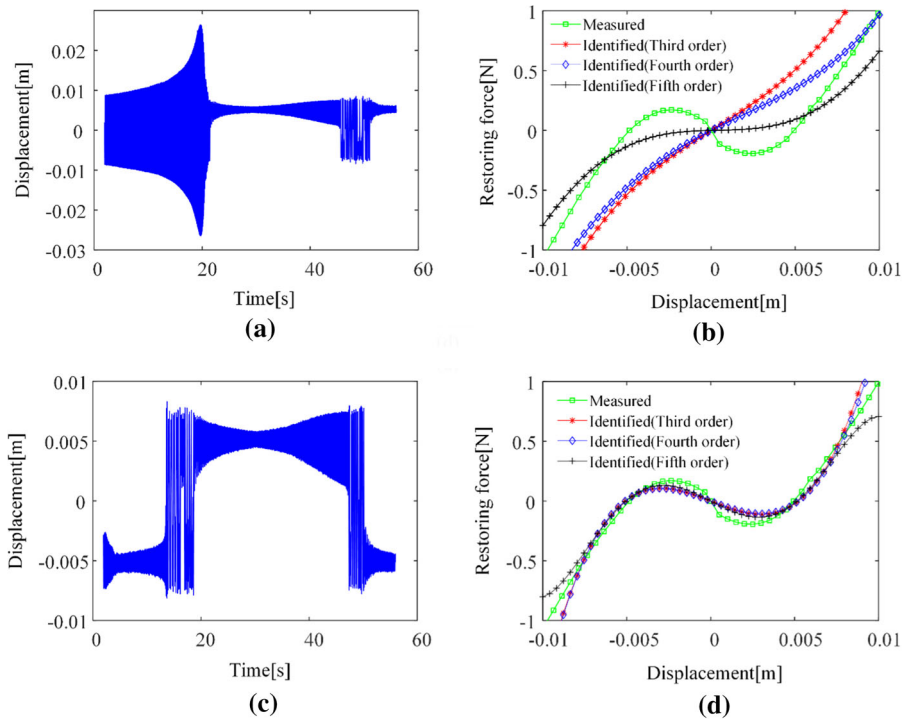

Fig. 11 Experimental data sets with a sampling frequency of 3125 Hz in a bistable piezoelectric cantilever beam. **a** Displacement response under the base acceleration of 5.5 m/s^2; **b** comparison between the identified nonlinear restoring force using the data sets (**a**) with different polynomial models; **c** displacement response under the base acceleration of 5 m/s^2; **d** comparison between the identified nonlinear restoring force using data sets (**c**) with different polynomial models and measured force–displacement curve

Table 4 RMS error of identified nonlinear restoring force curves

Order	Third	Fourth	Fifth
Error (%)	5.22	13.79	6.96

identification method can reduce the above-mentioned influence factors as much as possible.

To verify the effectiveness and accuracy of the proposed identification procedure, a typical bistable electromechanical coupling equation is adopted to perform numerical investigations. The essential linear mass, damping coefficient, linear stiffness and electromechanical coupling coefficient can be estimated even if 40 dB noise is added to the input and output simulation data. Firstly, for nonlinear restoring force identification in a bistable system, the frequency-swept response must contain inter-well and intra-well oscillations to ensure the identification accuracy and the possible explanations are discussed. Secondly, the influence of noise level on identification results indicates that identification accuracy will decrease obviously when the noise level is increased to 20 dB. Finally, experimental output responses of a magnetic coupled bistable piezoelectric cantilever beam are measured under different conditions for demonstrating the proposed method. The reconstructed dynamic responses of displacement and voltage based on identified basic parameters have a good consistency with the experimental data. The identified nonlinear restoring force is in good agreement with the quasi-static measured force–displacement curve. Moreover, the choice of polynomial order is significant in experimental conditions.

Acknowledgements This work is sponsored by the National Natural Science Foundation of China (Grant No. 51975453)

Availability of data and materials These data are collected by the experiment.

Code availability The code is written according to the proposed model.

Declarations

Conflict of interest The authors declare that they have no conflict of interest.

References

1. Harne, R.L., Wang, K.W.: Harnessing Bistable Structural Dynamics: For Vibration Control. Energy Harvesting and Sensing. Wiley, West Sussex (2017)
2. Erturk, A., Inman, D.J.: Broadband piezoelectric power generation on high-energy orbits of the bistable Duffing oscillator with electromechanical coupling. J. Sound Vib. **330**, 2339–2353 (2011)
3. Emam, S.A., Inman, D.J.: A review on bistable composite laminates for morphing and energy harvesting. Appl. Mech. Rev. **67**, 060803 (2015)
4. Leadenham, S., Erturk, A.: Unified nonlinear electroelastic dynamics of a bimorph piezoelectric cantilever for energy harvesting, sensing, and actuation. Nonlinear Dyn. **79**, 1727–1743 (2015)
5. Kim, P., Nguyen, M.S., Kwon, O., Kim, Y.J., Yoon, Y.J.: Phase-dependent dynamic potential of magnetically coupled two-degree-of-freedom bistable energy harvester. Sci. Rep. **6**, 34411 (2016)
6. Singh, K.A., Kumar, R., Weber, R.J.: A broadband bistable piezoelectric energy harvester with nonlinear high-power extraction. IEEE Trans. Power Electr. **30**, 6763–6774 (2015)
7. Lan, C., Tang, L., Qin, W., Xiong, L.: Magnetically coupled dual-beam energy harvester Benefit and trade-off. J. Intell. Mat. Syst. Str. **29**, 1216–1235 (2017)
8. Zhou, S.X., Cao, J.Y., Lin, J.: Enhanced broadband piezoelectric energy harvesting using rotatable magnets. Appl. Phys. Lett. **102**, 101301-R21 (2013)
9. Masana, R., Daqaq, M.F.: Electromechanical modeling and nonlinear analysis of axially loaded energy harvesters. J. Vib. Acoust. **133**, 011007.1-011007.10 (2011)
10. Zhang, J., Zhang, J., Shu, C., Fang, Z.: Enhanced piezoelectric wind energy harvesting based on a buckled beam. Appl. Phys. Lett. **110**, 3–468 (2017)
11. Hwang, M., Arrieta, A.F.: Input-independent energy harvesting in bistable lattices from transition waves. Sci. Rep. **8**, 3630 (2018)
12. Xia, Y., Ruzzene, M., Erturk, A.: Bistable attachments for wideband nonlinear vibration attenuation in a metamaterial beam. Nonlinear Dyn. **102**, 1–12 (2020)
13. Erturk, A., Hoffmann, J., Inman, D.: A piezomagnetoelastic structure for broadband vibration energy harvesting. Appl. Phys. Lett. **94**, 254102-254102–3 (2009)
14. Stanton, S.C., McGehee, C.C., Mann, B.P.: Nonlinear dynamics for broadband energy harvesting: investigation of a bistable piezoelectric inertial generator. Physica D **239**, 640–653 (2010)
15. Cao, J.Y., Zhou, S.X., Inman, D., Lin, J.: Nonlinear dynamic characteristics of variable inclination magnetically coupled piezoelectric energy harvesters. J. Vib. Acoust. **137**, 9 (2015)
16. Leadenham, S., Erturk, A.: M-shaped asymmetric nonlinear oscillator for broadband vibration energy harvesting: harmonic balance analysis and experimental validation. J. Sound Vib. **333**, 6209–6223 (2014)
17. Leadenham, S., Erturk, A.: Nonlinear M-shaped broadband piezoelectric energy harvester for very low base accelerations: primary and secondary resonances. Smart Mater. Struct. **333**, 6209–6223 (2015)
18. Masana, R., Daqaq, M.: Response of duffing-type harvesters to band-limited noise. J. Sound Vib. **332**, 6755–6767 (2013)
19. Stanton, S.C., Mann, B., Inman, D.: Nonlinear piezoelectricity in electroelastic energy harvesters: modeling and experimental identification. J. Appl. Phys. **108**, R175 (2010)
20. Zhou, S.X., Cao, J.Y., Inman, D., Lin, J., Liu, S., Wang, Z.: Broadband tristable energy harvester: modeling and experiment verification. Appl. Energy **313**, 33–39 (2014)
21. Yuan, T.C., Yang, J., Chen, L.Q.: Nonparametric identification of nonlinear piezoelectric mechanical systems. J. Appl. Mech. **85**, 1110081–11100813 (2018)
22. Yuan, T.C., Yang, J., Chen, L.Q.: Experimental identification of hardening and softening nonlinearity in circular laminated plates. Int. J. Non-Linear Mech. **95**, 296–306 (2017)
23. Nico, V., Frizzell, R., Punch, J.: Nonlinear analysis of a two-degree-of-freedom vibration energy harvester using high order spectral analysis techniques. Smart Mater. Struct. **26**, 045029 (2017)
24. Harris, P., Arafa, M., Litak, G., Bowen, C., Iwaniec, J.: Output response identification in a multistable system for piezoelectric energy harvesting. Eur. Phys. J. B **90**, 20 (2016)
25. Marchesiello, S., Garibaldi, L.: A time domain approach for identifying nonlinear vibrating structures by subspace methods. Mech. Syst. Signal Process. **22**, 81–101 (2008)
26. Noël, J.P., Kerschen, G.: Nonlinear system identification in structural dynamics: 10 more years of progress. Mech. Syst. Signal Process. **83**, 2–35 (2017)
27. Ghamami, M., Nahvi, H., Yaghoubi, V.: Automated modal parameters identification of bistable composite plate using two-stage clustering of operational modal testing. J. Compos. Mater. **1**, 1–14 (2020)
28. Mostafaei, H., Ghamami, M., Aghabozorgi, P.: Modal identification of concrete arch dam by fully automated operational modal identification. Structures **32**, 228–236 (2021)
29. Noël, J.P., Renson, L., Kerschen, G.: Complex dynamics of a nonlinear aerospace structure: experimental identification and modal interactions. J. Sound. Vib. **333**, 2588–2607 (2014)
30. Filippis, G.D, Noël, J.P., Kerschen, G., Soria, L., Stephan, C.: Experimental nonlinear identification of an aircraft with bolted connections. In: International Modal Analysis Conference (IMAC) XXXIII (2015)
31. Noël, J.P., Kerschen, G.: Frequency-domain subspace identification of nonlinear mechanical systems—application to a solar array structure. Mech. Syst. Signal Process. **40**, 701–717 (2013)
32. Liu, J., Li, B., Miao, H., Zhang, X., Li, M.: A modified time domain subspace method for nonlinear identification based

on nonlinear separation strategy. Nonlinear Dyn. **94**, 1–19 (2018)
33. Zhang, M.W., Wei, S., Peng, Z., Dong, X.J., Zhang, W.: A two-stage time domain subspace method for identification of nonlinear vibrating structures. Int. J. Mech. Sci. **120**, 81–90 (2017)
34. Anastasio, D., Marchesiello, S., Kerschen, G., Noël, J.P.: Experimental identification of distributed nonlinearities in the modal domain. J. Sound. Vib. **458**, 426–444 (2019)
35. Adams, D.E., Allemang, R.J.: A frequency domain method for estimating the parameters of a non-linear structural dynamic model through feedback. Mech. Syst. Signal Process. **14**, 637–656 (2000)
36. Overschee, P.V., Moor, B.D.: Subspace identification for linear systems. Springer, Boston (1996)
37. Overschee, P. V., Moor, B. D.: N4SID: numerical algorithms for state space subspace system identification. In: Proceedings of the World Congress of the International Federation of Automatic Control, vol. 7, pp. 361–364 (1993)
38. Verhaegen, M.: Identification of the deterministic part of MIMO state space models given in innovations form from input–output data. Automatica (Special Issue on Statistical Signal Processing and Control) **30**, 61–74 (1994)
39. Wei, S., Peng, Z.K., Dong, X.J., Zhang, W.M.: A nonlinear subspace-prediction error method for identification of nonlinear vibrating structures. Nonlinear Dyn. **91**, 1605–1617 (2018)
40. Reynders, E., Roeck, G.D.: Reference-based combined deterministic-stochastic subspace identification for experimental and operational modal analysis. Mech. Syst. Signal Process. **22**, 617–637 (2008)
41. Wang, W., Cao, J.Y., Bowen, C.R., Zhang, Y., Lin, J.: Nonlinear dynamics and performance enhancement of asymmetric potential bistable energy harvesters. Nonlinear Dyn. **94**, 1183–1194 (2018)
42. Zhou, Z., Qin, W., Zhu, P.: Harvesting performance of quad-stable piezoelectric energy harvester: modeling and experiment. Mech. Syst. Signal Process. **110**, 260–272 (2018)
43. Zhang, Y., Cao, J.Y., Wang, W., Liao, W.H.: Enhanced modeling of nonlinear restoring force in multi-stable energy harvesters. J. Sound. Vib. **494**, 115890 (2021)